The Astrophysical Journal, 730:16 (7pp), 2011 March 20 doi:10.1088/0004-637X/730/1/16

THE STRUCTURE OF THE ACCRETION DISK IN THE LENSED QUASAR SBS 0909+532

E. Mediavilla[1,2], J. A. Muñoz[3], C. S. Kochanek[4], E. Guerras[1,2], J. Acosta-Pulido[1,2], E. Falco[5], V. Motta[6], S. Arribas[7], A. Manchado[1,2], and A. Mosquera[3,4]

[1] Instituto de Astrofísica de Canarias, Vía Láctea S/N, La Laguna 38200, Tenerife, Spain
[2] Departamento de Astrofísica, Universidad de la Laguna, La Laguna 38200, Tenerife, Spain
[3] Departamento de Astronomía y Astrofísica, Universidad de Valencia, 46100 Burjassot, Valencia, Spain
[4] Department of Astronomy and the Center for Cosmology and Astroparticle Physics, The Ohio State University, 4055 McPherson Lab, 140 West 18th Avenue, Columbus, OH 43221, USA
[5] Center for Astrophysics, 60 Garden Street, Cambridge, MA 02138, USA
[6] Universidad de Valparaíso, Avda. Gran Bretaña 1111, Playa Ancha, Valparaíso, Chile
[7] Departamento de Astrofísica, Centro de Astrobiología (CSIC-INTA), Crta. Ajalvir Km. 4, 28850 Torrejon de Ardoz, Madrid, Spain
Received 2010 August 30; accepted 2011 January 14; published 2011 February 24

ABSTRACT

We derive the size and temperature profile of the accretion disk of the lensed quasar SBS 0909+532 by measuring the wavelength dependence (chromaticity) of the microlensing magnification produced by the stars in the lens galaxy. After correcting for extinction using the flux ratios of 14 emission lines, we observe a marked change in the B–A flux ratio with wavelength, varying from -0.67 ± 0.05 mag at (rest frame) ∼1460 Å to -0.24 ± 0.07 mag at ∼6560 Å. For $\lambda \gtrsim 7000$ Å both effects, extinction and microlensing, look minimal. Simulations indicate that image B rather than A is strongly microlensed. If we model the change in disk size from 1460 Å to 6560 Å using a Gaussian source ($I \propto \exp(-R^2/2r_s^2)$) with a disk size scaling with wavelength as $r_s \propto \lambda^p$, we find $r_s = 7^{+5}_{-3}$ light-days at 1460 Å and $p = 0.9^{+0.6}_{-0.3}$ for uniform priors on r_s and p, and $r_s = 4^{+3}_{-3}$ light-days and $p = 1.0^{+0.6}_{-0.4}$ for a logarithmic prior on r_s. The disk temperature profile $T \propto R^{-1/p}$ is consistent with thin disk theory ($T \propto R^{-3/4}$), given the uncertainties. The estimates of r_s are also in agreement with the size inferred from thin disk theory using the estimated black hole mass ($M_{\rm BH} \simeq 2 \times 10^9\, M_\odot$) but not with the smaller size estimated from thin disk theory and the optical flux. We also use the flux ratios of the unmicrolensed emission lines to determine the extinction curve of the dust in the lens galaxy, finding that it is similar to that of the LMC2 Supershell.

Key words: dust, extinction – gravitational lensing: micro – quasars: individual (SBS 0909+532)

1. INTRODUCTION

The high efficiency with which active galactic nuclei (AGNs) and quasars generate energy leads almost inescapably to the existence of a mechanism for transferring matter into the deep gravitational well of a supermassive black hole (Zel'dovich 1964; Salpeter 1964). A simple, commonly used model based on this hypothesis is the thin accretion disk model (Shakura & Sunyaev 1973), which predicts, among other physical parameters of interest, the size of the disk and the radial dependence of its surface temperature. Observational studies of the accreting region to test these predictions are, unfortunately, very limited due to the small angular size of accretion disks. Until recently, most observational studies relied on indirect evidence based on variability (see, e.g., Sergeev et al. 2005) or models of spectral energy distributions (SEDs; see Bonning et al. 2007 and references therein). The detection of extremely broad FeKα X-ray emission lines in a few AGNs and quasars opened a more direct approach to the study of the inner region of the accreting disk and its potentially exotic physics (Fabian 2005), but the observations are very challenging.

Multiply imaged quasars offer at least two ways to resolve the accretion structure using the microlensing of the disk by the stars in the lens galaxy (quasar microlensing; Chang & Refsdal 1979; see also the review by Wambsganss 2006). The first is through time variability, using the amplitude and rate of the variability to constrain the disk size (Rauch & Blandford 1991; Jaroszynski et al. 1992; Yonehara et al. 1998). With this approach, the challenge is obtaining the necessary monitoring data, but given the data there is a well-established analysis method (Kochanek 2004). Disk size measurements based on variability are now routine (e.g., Morgan et al. 2010) and can even be used to study disk inclinations (Poindexter & Kochanek 2010). The second approach is through the wavelength dependence of the microlensing. If, as predicted by the thin disk model, the size of the emitting region varies with wavelength, then the microlensing magnification should be wavelength dependent. Measuring the SED of the lensed images at a single epoch can reveal this microlensing "chromaticity" and by modeling it both the size and the temperature profile of the source can be constrained. Many recent studies have used this approach (Pooley et al. 2007; Anguita et al. 2008; Agol et al. 2009; Bate et al. 2008; Floyd et al. 2009; Blackburne et al. 2010), although care is required to distinguish between microlensing chromaticity and differential extinction. This can be done relatively easily by using the unmicrolensed emission line flux ratios to determine the extinction and then correct the continuum flux ratios before carrying out the microlensing analysis (see, e.g., Mediavilla et al. 2009). The two approaches can also be combined, as in the studies by Poindexter et al. (2008), Morgan et al. (2008), or Dai et al. (2010).

There are not many studies of microlensing chromaticity based on the measurements of the offsets between the continuum and emission line flux ratios. In HE 1104−1805, Wisotzki et al. (1993, 1995) found that the continuum flux ratio between the two images depended on wavelength but the flux ratios were approximately constant for the emission lines. In HE 0512−3329, Wucknitz et al. (2003) used the emission lines to separate the extinction and microlensing-induced chromaticities. In Q 2237+0305, Mosquera et al. (2009) used narrowband imaging

rather than spectroscopy to separate the emission lines from the continuum and detected chromatic microlensing in image A. In the two-image lens SBS 0909+532 ($z_l = 0.83$, $z_s = 1.38$) we had previously noticed the different flux ratios in the lines and continuum (Motta et al. 2002, also see Oscoz et al. 1997) and in Mediavilla et al. (2005) we found that these differences continued into the ultraviolet (UV). Here we extend these results into the near-IR and combine them to determine both the structure of the accretion disk and the extinction law of the dust in the lens galaxy. The paper is organized as follows. In Section 2 we present the new IR data and derive the magnitude differences (created by microlensing and extinction) as a function of wavelength. In Sections 3.1 and 3.2 we use the effects of microlensing to study the structure of the accretion disk, and in Section 3.3 we determine the extinction curve of the dust in the lens galaxy using the parameterization of Fitzpatrick & Massa (1990). Finally, in Section 4 we summarize the main conclusions.

2. DATA

We obtained near-IR spectra using the LIRIS instrument mounted on the 4.2 m William Herschel Telescope (WHT) at the Observatorio del Roque de los Muchachos on the nights of 2004 March 5 and 2005 January 22, as part of the LIRIS Guaranteed Time program. LIRIS is an infrared camera/spectrograph built at the Instituto de Astrofisica de Canarias (Manchado et al. 2004). In 2004 March we obtained a spectrum using the ZJ grism (0.9–1.5 μm and R 500), a slit width of 1.″0, and a total exposure time of 2000 s split into four exposures of 500 s each. In 2005 January we obtained a spectrum using the HK grism (1.5–2.4 μm and R 650), a slit width of 0.″75, and a total exposure time of 1800 s split into six exposures of 300 s each. Both observations were performed using an ABBA telescope nodding pattern and with the slit oriented at the position angle (PA) defined by the two quasar images. The measurements were taken using multiple correlated readout mode, including four readouts before and after the integration to reduce the readout noise. The nearby A2 star HD 784888 was observed with the same configuration to make the telluric corrections and for flux calibration.

The data were reduced and calibrated using the package "lirisdr," developed by the LIRIS team within the IRAF environment. Consecutive pairs of AB frames were subtracted to remove the sky background, then the resulting images were wavelength calibrated and flat-fielded. All resulting frames were registered and co-added to provide the final combined spectrum. Then, the one-dimensional spectra of the two quasar images were extracted and divided by a composite spectrum to remove telluric absorption. This composite spectrum was generated from the observed spectra of the calibration star, divided by a stellar model of the same spectral type that was smoothed to our spectral resolution.

We merged these near-IR spectra with the UV and optical spectra from our earlier studies. The optical spectrum was obtained with the fiber system *INTEGRAL* (Arribas et al. 1998) at the WHT on 2001 January 18 (Motta et al. 2002) and the UV spectrum was obtained with Space Telescope Imaging Spectrograph (STIS) on the *Hubble Space Telescope* (*HST*) on 2003 March 7 (Mediavilla et al. 2005). We merged the previously joined optical/UV composite spectrum to the new Z/J-band spectra using the overlap at 8958–9245 Å. The normalization factors were 1.00 ± 0.02 and 0.91 ± 0.02 for the A and B components, respectively. There is no direct overlap of the H/K spectra with the other data, so we fit a power law

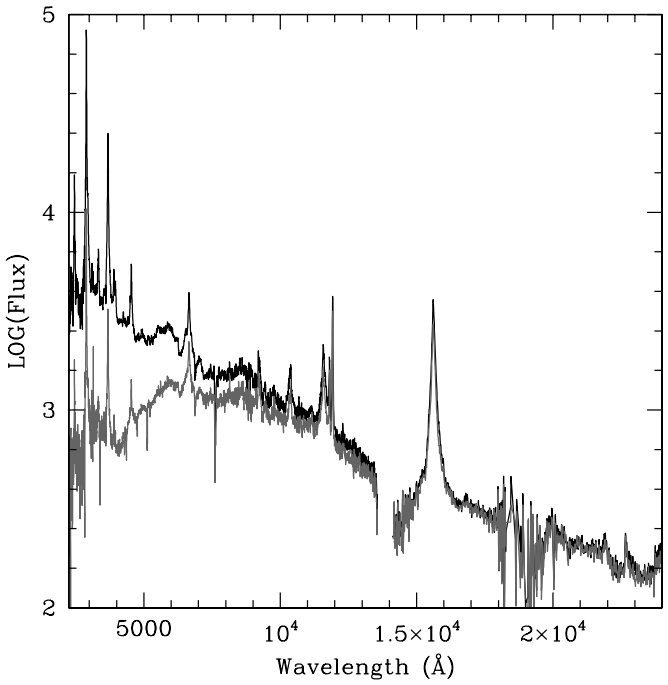

Figure 1. STIS+INTEGRAL+LIRIS spectra corresponding to A (black) and B (gray) images of SBS 0909+532. The flux scale is in arbitrary units.

to the A spectrum in the wavelength range ~8000–12900 Å, and used its extrapolation to match the H/K spectrum in the wavelength range ~18200–22900 Å. The merged spectrum is shown in Figure 1. Note the prominent Hα + [N II] blend in the H band.

Figure 2 shows the flux ratio between the spectra of the two quasar images as a magnitude difference, where we have smoothed the spectrum with a Gaussian filter of $\sigma = 1.5$ Å to reduce the noise fluctuations. We clearly see significant differences between the continuum and emission line regions, particularly in the UV. To separate the two emission components we subtracted a linear model for the continuum from each emission line, determined by fits to the continuum regions adjacent to each emission line, and measured an average line flux ratio. Away from the lines we smoothed the continuum in intervals of roughly 400 Å, to estimate the continuum flux ratios. These line and continuum flux ratios are also shown in Figure 2, and we clearly see the significant offsets between the continuum and emission lines created by microlensing, as we had previously noted in Motta et al. (2002) and Mediavilla et al. (2005), and that the offset steadily decreases as we approach the near-IR.

For comparison we show the B, V, R, I, and H broadband magnitude differences from Kochanek et al. (1997) and Lehár et al. (2000). The general agreement of these flux ratios with the spectroscopic results despite the significant time separations suggests that we need worry little about the time variability created by microlensing in merging the optical, UV, and near-IR spectra. We also note that the time delay in SBS 0909+532 should be short enough (Lehár et al. 2000) that we need not be concerned about intrinsic variability modulated by the time delay contaminating the flux ratios. Unfortunately, we have no tests for these effects at the shortest wavelengths.

To isolate the microlensing effects we measure the offsets between the continuum and line flux ratios, $\Delta m = (m_B - m_A)_{con} - (m_B - m_A)_{lin}$. This is based on the assumption

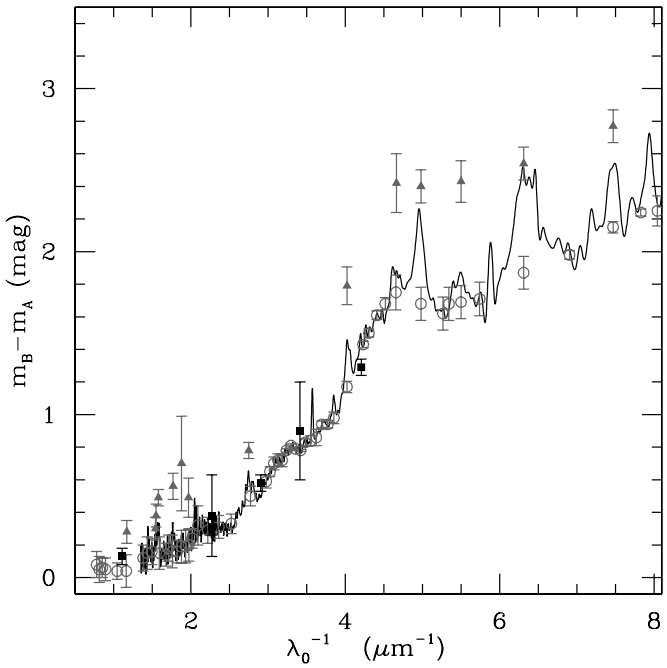

Figure 2. Continuous curve shows the magnitude difference of the merged STIS+INTEGRAL+LIRIS spectra. Gray circles (continuum) and triangles (emission line) correspond to integrated magnitude differences (see the text). Black squares correspond to broadband photometry from the literature (see the text).

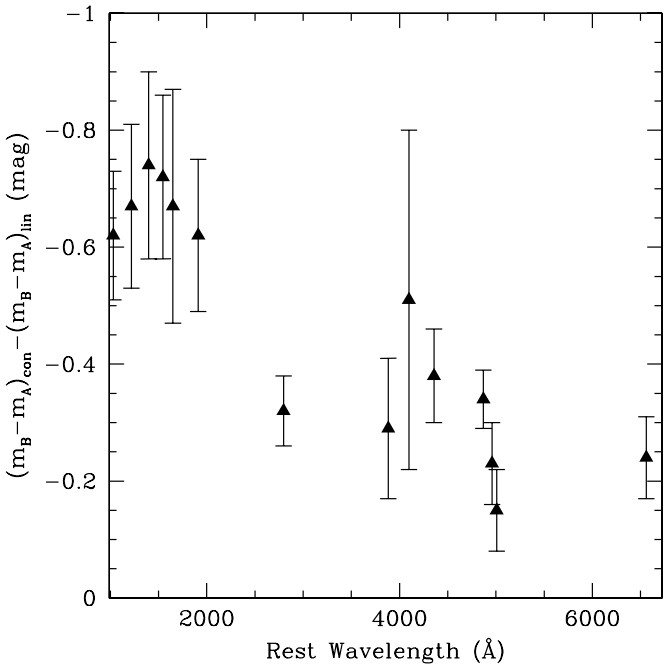

Figure 3. Wavelength dependence of the difference between the continuum and emission line flux ratios for the (from blue to red) Lyβ, Lyα, Si IV + O IV], C IV, He II + O III], C III], Mg II, He I, Hδ, Hγ, Hβ, [O III]λ4959, [O III]λ5007, and Hα + [N II] emission lines.

that the emission line regions are much larger than the regions that can be significantly microlensed.[8] Figure 3 shows the estimates of Δm associated with each of the emission lines (Lyβ, Lyα, Si IV + O IV], C IV, He II + O III], C III], Mg II, He I, Hδ, Hγ, Hβ, [O III]λ4959, [O III]λ5007, and Hα + [N II]; from blue to red). We see that Δm shifts with wavelength. B is considerably brighter in the UV but becomes comparable to A in the optical/near-IR, with a chromatic change of $\sim$0.5 magnitudes between the amplitude at 6600 Å and 1500 Å. Note that the offset remains even at the wavelength of Hα.

In principle, we may use the 14 data points in Figure 3 in our posterior simulations. However, this would imply a huge computational effort that is not justified by the uncertainties. To quantify the dependence of the microlensing amplitude on wavelength, we will take an average value from the six bluest emission lines,

$$\Delta m_1^{\rm obs}(\lambda_1 \sim 1459 \pm 314\ \text{Å}) = -0.67 \pm 0.05, \quad (1)$$

an intermediate value corresponding to the average of the microlensing amplitudes associated with the seven intermediate wavelength emission lines,

$$\Delta m_2^{\rm obs}(\lambda_2 \sim 4281 \pm 789\ \text{Å}) = -0.30 \pm 0.10, \quad (2)$$

and the value associated with the reddest emission line:

$$\Delta m_3^{\rm obs}(\lambda_3 \sim 6559\ \text{Å}) = -0.24 \pm 0.07. \quad (3)$$

The uncertainties in the averaged wavelengths are the rms dispersions.

[8] No significant microlensing magnification is expected for the narrow emission lines and for the low ionization broad emission lines, especially if the lensed source is a bright quasar. However, microlensing could affect the high ionization broad lines of low-luminosity AGNs (Abajas et al. 2002).

3. DISCUSSION

3.1. Microlensing and the Structure of the Accretion Disk

We model the accretion disk as a Gaussian intensity profile $I(R) \propto \exp(-R^2/2r_s^2)$ characterized by a wavelength-dependent size r_s. By randomly placing such a source on microlensing magnification maps corresponding to the A and B images of SBS 0909+532, we can estimate the probability of reproducing the flux ratios measured in Section 2 ($\Delta m_l^{\rm obs}(\lambda_l)$, $l = 1, 2, 3$). The model depends on seven parameters: the convergence and shear corresponding to each image (κ_A, γ_A, κ_B, γ_B), the mass fraction in microlenses (α), the accretion disk size at 1459 Å (r_s), and the power-law index (p) relating the disk sizes at different wavelengths ($r_s(\lambda) \propto \lambda^p$).

The four macrolens parameters (κ_A, γ_A, κ_B, γ_B) are fixed by a simple, standard model of the lens system. We used a singular isothermal sphere (SIS) in an external shear field to fit the relative separations of the two lensed images and the lens galaxy, using the CASTLES[9] *HST* astrometry. In general, it is risky to constrain models with flux ratios because of the combined effects of microlensing, substructure, and extinction (Kochanek 2006), but here with our large wavelength coverage (Figures 1 and 2) these effects are minimal for (rest-frame) wavelengths $\lambda \gtrsim 7000$ Å, so averaging in this region the continuum magnitudes difference we adopt a flux ratio constraint of $m_B - m_A = 0.05 \pm 0.05$ mag. The resulting values for the convergence and shear at the locations of the images are (κ_A, γ_A) = (0.66, 0.70) and (κ_B, γ_B) = (0.36, 0.25). We then considered models in which a fraction $\alpha = 2^{-i}$ with $i = 0, \ldots, 6$ of the surface density is comprised of stars and the remainder is smoothly distributed dark matter. All stars were given a common mass of $M = M_\odot$. From the source $z_s = 1.38$ and lens $z_l = 0.83$ redshifts the source plane Einstein radius is

[9] Cfa-Arizona Space Telescope LEns Survey (www.cfa.harvard.edu/castles/).

$R_E = 3.3 \times 10^{16}(M/M_\odot)^{1/2}$ cm (=12.6$(M/M_\odot)^{1/2}$ light-days) for an $\Omega_0 = 0.3, \Lambda_0 = 0.7, h = 0.7$ flat cosmological model. For each value of α_i we compute magnification maps of $80 \times 80\ R_E^2$ (2000×2000 pixels^2) for both images using the Inverse Polygon Method (Mediavilla et al. 2006). We convolved the maps with the Gaussians representing the disk structure. For r_s we consider both a linear grid $r_{sj}(1459\ \text{Å}) = 1, 2, \ldots, 30$ light-days and a logarithmic grid $\log r_{sj}(1459\ \text{Å}) = ((\log 30)/29) \cdot (j-1)$ light-days ($j = 1, 2, \ldots, 30$) better suited for the use of a logarithmic prior. For p we consider the linear grid $p_k = 0.0, 0.1, \ldots, 2.1$. Thus, the size at λ_l is $r_{sjk}(\lambda_l) = r_{sj}(1459\ \text{Å})(\lambda_l/1459\ \text{Å})^{p_k}$. After convolution we normalized each $\mu_{ijklA,B}$ magnification map by its mean value so that the difference magnification maps (expressed in magnitudes)

$$\Delta\mu_{ijkl} = \mu_{ijklA} - \mu_{ijklB} \tag{4}$$

determine the relative microlensing magnifications of images A and B. For each case, we randomly sample the patterns to build a histogram of events $N_{ijk}(\Delta m_1, \Delta m_2, \Delta m_3)$. We calculate 4620 histograms with 10^8 events in each. The probability of the data given the model is then

$$p\left(\Delta m_1^{\rm obs}, \Delta m_2^{\rm obs}, \Delta m_3^{\rm obs} \middle| \alpha_i, r_{sj}, p_k\right) \propto \int d\Delta m_1 \int d\Delta m_2 \int d\Delta m_3 N_{ijk} e^{-\frac{1}{2}\chi^2}, \tag{5}$$

where

$$\chi^2 = \sum_{l=1}^{3} \frac{\left(\Delta m_l - \Delta m_l^{\rm obs}\right)^2}{\sigma^2_{\Delta m_l^{\rm obs}}}. \tag{6}$$

We find many cases with statistically acceptable values for χ^2, and the results do not change significantly if we restrict the calculations in Equation (5) to cases with $\chi^2 < 3$.

Using Bayes' theorem, the probability of the parameters given the data is then

$$p\left(\alpha_i, r_{sj}, p_k \middle| \Delta m_1^{\rm obs}, \Delta m_2^{\rm obs}, \Delta m_3^{\rm obs}\right) \propto p\left(\Delta m_1^{\rm obs}, \Delta m_2^{\rm obs}, \Delta m_3^{\rm obs} \middle| \alpha_i, r_{sj}, p_k\right) p(\alpha_i, r_{sj}, p_k), \tag{7}$$

where $p(\alpha_i, r_{sj}, p_k)$ represents the priors on the model parameters and the overall normalization is such that $\sum_{ijk} p(\alpha_i, r_{sj}, p_k | \Delta m_1^{\rm obs}, \Delta m_2^{\rm obs}, \Delta m_3^{\rm obs}) \equiv 1$.

The present data do not constrain the stellar mass fraction, α. Fortunately, the estimates of the disk structure are little affected by this for reasonable values of $\alpha \lesssim 0.3$. In any case, we used as a prior for α the likelihood function $L(\alpha)$ derived by Mediavilla et al. (2009) from a statistical survey of microlensing in quasars, which favors low stellar mass fractions, $0.02 \lesssim \alpha \lesssim 0.14$, as might be expected in the region near the lensed images. To analyze the sensitivity of our study to the treatment of the size prior (see Morgan et al. 2010), we have considered two priors, linear and logarithmic, for r_s.

Summing on α_i we obtain the marginalized probability density function for r_s and p,

$$p\left(r_{sj}, p_k \middle| \Delta m_1^{\rm obs}, \Delta m_2^{\rm obs}, \Delta m_3^{\rm obs}\right) = \sum_i p\left(\alpha_i, r_{sj}, p_k \middle| \Delta m_1^{\rm obs}, \Delta m_2^{\rm obs}, \Delta m_3^{\rm obs}\right). \tag{8}$$

In Figure 4, we show this marginalized probability density function for both linear and logarithmic grids in r_s. There is an (anti-)covariance (more marked in the plot with a logarithmic grid in r_s) between r_s and p. Note that the computation of an expected value or confidence interval integrating on dr_s ($d \log r_s$) will be equivalent to the use of a linear (logarithmic) prior. We obtain estimates for the source parameters of $r_s(1459\ \text{Å}) = 8^{+5}_{-4}$ light-days, $p = 0.9^{+0.6}_{-0.3}$ and $r_s(1459\ \text{Å}) = 5^{+4}_{-3}$ light-days, $p = 1.0^{+0.6}_{-0.4}$ for the linear and logarithmic priors, respectively. As far as there are not a priori reasons to prefer one or other prior, the difference between the two estimates for r_s should be regarded as a test of the sensitivity of the method to the prior.

Microlensing magnification patterns can be qualitatively described by a series of complex high magnification ridges of caustics separated by relatively smooth valleys of demagnification. If we examine the origin of the chromaticity in detail for the case $\alpha = 0.125$, $p = 0.8$, and $r_s = 8$ light-days, we find that they are generally (90%) due to image B lying close to a caustic with A in a relatively smooth region of the magnification patterns rather than the reverse or having both images lying either in ridges or valleys.

3.2. Comparison with the Standard Thin Disk Model

The radial dependence of the surface temperature in the accretion disk is obtained equating the local radiation energy flux to the gravitational energy release (Shakura & Sunyaev 1973). When the local spectrum of the thermal radiation is a Planck distribution, a $T \propto R^{-\beta}$ law with $\beta = 3/4$ is obtained. Defining the radius at which the disk temperature matches the wavelength, R_λ, from $kT(R_\lambda) = hc/\lambda$, a size scaling $R_\lambda \propto \lambda^p$ with $p = 1/\beta = 4/3$ is derived. From our microlensing data we derive a compatible estimate, $p = 0.9^{+0.6}_{-0.3}$. Excepting Floyd et al. (2009; see also Blackburne et al. 2010), other microlensing estimates based on multi-band observations (Eigenbrod et al. 2008; Poindexter et al. 2008; Anguita et al. 2008; Bate et al. 2008; Mosquera et al. 2009) are also compatible with the $T \propto R^{-3/4}$ law within their uncertainties (see Floyd et al. 2009; Morgan et al. 2010).

The energy condition locally equating blackbody radiation and gravitational energy release provides an estimate of R_λ (Shakura & Sunyaev 1973),

$$R_\lambda = 9.7 \times 10^{15} \left(\frac{\lambda}{\mu\text{m}}\right)^{4/3} \left(\frac{M_{\rm BH}}{10^9\ M_\odot}\right)^{2/3} \left(\frac{L}{\eta L_E}\right)^{1/3} \text{cm}, \tag{9}$$

where η is the radiative efficiency, $L = \eta \dot{M} c^2$ is the luminosity, and L_E is the Eddington luminosity. In our case, $\lambda_{\rm rest} = 1500$ Å. Based on the Mg II line, Peng et al. (2006) estimated a black hole mass of $M_{\rm BH} \simeq 10^{9.59}\ M_\odot$ while based on the C IV, Hβ, and Hα lines, Assef et al. (2010) estimate masses of $10^{8.51}$, $10^{9.29}$, and $10^{9.15}\ M_\odot$, respectively. The difference between the C IV and Hβ estimates is largely explained by the correlation of the mass differences with the UV/optical spectral slope discovered in that paper. Adopting the Hβ mass estimate, $L/L_E \sim 1$ and $\eta \sim 0.1$, the estimated radius enclosing half of the luminosity is $R_{1/2} = 2.44 R_\lambda = 2.4$ light-days. This result assumes $\beta = 3/4$ ($p = 4/3$). We lack an alternative disk model with $p \sim 1$, so we cannot generalize Equation (9) to this case. If we fix $p = 4/3$ in our simulations, we find sizes of $R_{1/2} = 1.18 r_s = 6^{+4}_{-2}$ light-days (linear prior) and $R_{1/2} = 4^{+3}_{-2}$ light-days (logarithmic prior) in agreement with the estimate derived from Equation (9) given the uncertainties.

On the other hand, we can also estimate R_λ from the observed flux at some wavelength, F_ν. The luminosity of the accretion disk at wavelength λ can be obtained integrating the local

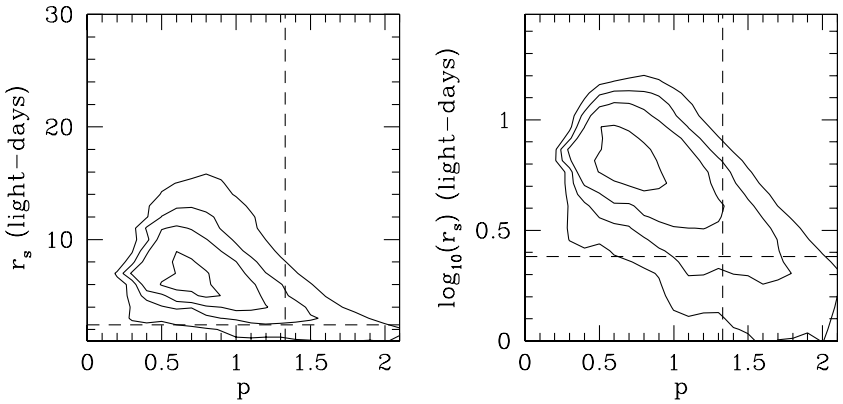

Figure 4. Probability density functions for the linear (left) and logarithmic (right) size priors. Contours correspond to 15%, 47%, 68%, and 90% of enclosed probability. Vertical dashed lines correspond to the thin disk theoretical value for the scaling index ($p = 1/\beta = 4/3$). Horizontal dashed lines correspond to the size inferred from thin disk theory using the estimated black hole mass (see the text).

spectrum of the radiation, $f_\nu(T(R))$, over radius,

$$L_\nu = \int_0^\infty f_\nu(T(R))2\pi R(\cos i)dR, \tag{10}$$

where i is the disk inclination. When f_ν is the Planck spectrum and $T \propto R^{-3/4}$, we obtain

$$R_\lambda = \sqrt{\frac{3/4}{\Gamma(\frac{8}{3})\zeta(\frac{8}{3})}}\sqrt{\frac{1}{hc}}\sqrt{\frac{1}{\cos i}}D_{\rm OS}\lambda_{\rm obs}^{3/2}\sqrt{F_\nu}, \tag{11}$$

where Γ and ζ are the Gamma and Riemann ζ functions and $D_{\rm OS}$ is the angular distance between observer and source. For the I band this implies

$$R_\lambda = 2.83\times10^{15}\sqrt{\frac{1}{\cos i}}\frac{D_{\rm OS}}{r_H}\left(\frac{\lambda_{\rm obs}}{\mu{\rm m}}\right)^{3/2}10^{-0.2(I_0-19)}h^{-1}\,{\rm cm} \tag{12}$$

(Morgan et al. 2008; Dai et al. 2010), where r_H is the Hubble radius ($r_H = c/H_0$), $\lambda_{\rm obs}$ is the observed wavelength (0.814 μm for the I filter), and I_0 is the intrinsic flux (in magnitudes) at $\lambda_{\rm obs}$. Here we must estimate the source flux, I_0, in the presence of high extinction and microlensing. For a double lens like SBS 0909+532, two equations can be written to derive I_0,

$$I_0 = I_{\rm A} - \mu_{\rm A} - A_{\rm A} - \Delta\mu_{\rm A} \tag{13}$$

and

$$I_0 = I_{\rm B} - \mu_{\rm B} - A_{\rm B} - \Delta\mu_{\rm B}, \tag{14}$$

where $I_{\rm A,B}$, $\mu_{\rm A,B}$, $A_{\rm A,B}$, and $\Delta\mu_{\rm A,B}$ are the observed fluxes (in magnitudes), the macrolens magnifications, the extinctions, and the microlensing magnifications for each image of the quasar. From CASTLES we obtain $I_{\rm A} = 16.23$ and $I_{\rm B} = 16.61$. The macrolens magnifications inferred from our SIS+γ model are $\mu_{\rm A} = \mu_{\rm B} = -1.14$. From the emission line ratio at 0.814 μm (see Figure 2) we infer $A_{\rm B} - A_{\rm A} = 0.8$. Finally, from the difference between the emission line and continuum ratios at 0.814 μm (Figure 3) we obtain $\Delta\mu_{\rm B} - \Delta\mu_{\rm A} = -0.4$. If we assume (see Figure 1) that there is extinction only for image B ($A_{\rm B} \gg A_{\rm A} \sim 0$) and that B is significantly magnified by microlensing while A suffers little demagnification ($\Delta\mu_{\rm B} \ll \Delta\mu_{\rm A} \sim 0$), then from Equations (13) and (14) we find $I_0 \sim 16.97$ and $I_0 \sim 16.95$ for images A and B, respectively.

Using $I_0 = 16.96$ and $\cos i = 1/2$ in Equation (12), we derive $R_{1/2} = 2.44R_\lambda = 2.9$ light-days for $\lambda_{\rm rest} = 0.342\,\mu$m. If we scale to other wavelengths assuming $p = 4/3$, we find $R_{1/2} = 0.95$ light-days at $\lambda_{\rm rest} = 0.150\,\mu$m. This value is smaller by a factor of ~ 3 than the size based on the black hole mass, $R_{1/2} = 2.4$ light-days (Equation (9)) and smaller than the microlensing size estimates obtained for $p = 4/3$: $R_{1/2} = 6^{+4}_{-2}$ light-days (linear prior) and $R_{1/2} = 4^{+3}_{-2}$ light-days (logarithmic prior). This discrepancy is similar to that found by Pooley et al. (2007), Morgan et al. (2010), and Blackburne et al. (2010). The discrepancies can be reduced by making p substantially larger than 4/3 corresponding to a shallower temperature profile (Poindexter et al. 2008; Morgan et al. 2010). A value $p = 1/\beta \geqslant 2$ is needed to bring the different sizes into agreement within uncertainties. However, the available microlensing estimates (Floyd et al. 2009; Morgan et al. 2010; Blackburne et al. 2010) predict $p \leqslant 1.65$, with an average value (Morgan et al. 2010 and the present work) of $\langle p\rangle = 1.2 \pm 0.3$. In the framework of the thin disk model, the value $\beta = 1/2$ corresponds to the limiting case where local energy generation from accretion plays no role in the heating at a given radius (Gaskell 2008). Although contamination from larger physical scales due to scattering or emission lines could also help to alleviate the flux size problem (Morgan et al. 2010), it is clear that more complex disk models should also be explored. For example, changes from a thermal radiation spectrum would, in general, imply $p \neq 1/\beta$, so $p \sim 1$ would not necessarily imply a temperature profile steeper than 4/3.

3.3. NIR–Optical–FUV Extinction Curve

With the new near-IR spectra, we can also study the NIR–Optical–FUV extragalactic extinction curve with unprecedented wavelength coverage. We do so using the differential extinction between the two images created by their different paths through the lens galaxy (Nadeau et al. 1991). The problem is that microlensing also modifies the continuum slopes. In principle, we could simply fit the differential magnitude curve defined by the emission lines since these are not affected by microlensing. However, the UV bump is poorly constrained because there are few lines in the 2175 Å region. It is preferable to estimate the bump parameters from the continuum data assuming that the impact of the microlensing on this determination is negligible. Thus, we modeled the line and continuum simultaneously, where for the lines (see, e.g., Falco et al. 1999; Muñoz et al. 2004),

$$\Delta m(\lambda_i) = a_0 + \Delta E(B-V)R_{\lambda_i}, \tag{15}$$

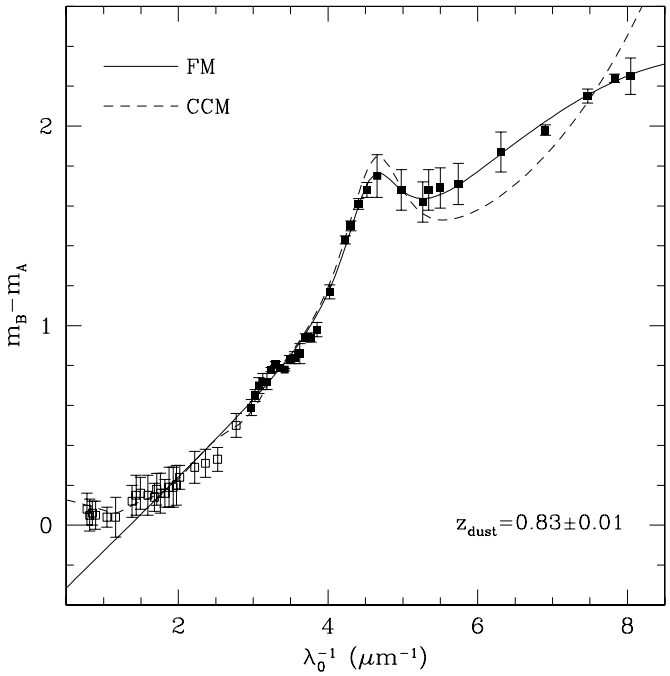

Figure 5. Fitzpatrick & Massa (1990, FM, solid line) and Cardelli et al. (1989, CCM, dashed line) model fits without considering microlensing chromaticity ($b_1 \equiv b_2 \equiv 0$; see the text) to the continuum flux ratios (squares). We have not considered the near-IR data (open squares) to fit the FM model (for it is simply $\propto \lambda^{-1}$ in this region).

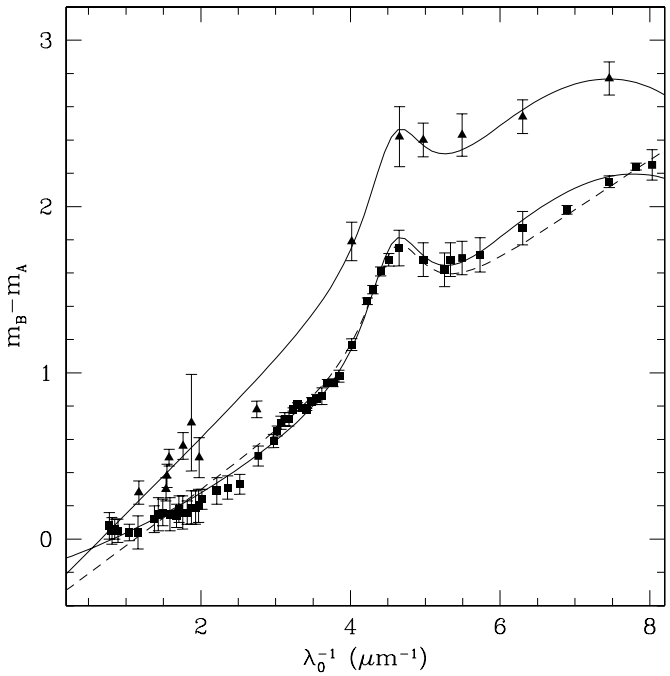

Figure 6. Solid lines: Fitzpatrick & Massa (1990, FM) combined fit to the continuum (squares) and emission lines (triangles) flux ratios using a second order polynomial in λ^{-1} to model the continuum chromaticity induced by microlensing (see the text). A fit using the same model but considering exclusively the continuum data is included for comparison (dashed line).

while for the continuum,

$$\Delta m(\lambda) = b_0 + b_1\lambda^{-1} + b_2\lambda^{-2} + \Delta E(B-V)R_{\lambda_i}, \qquad (16)$$

where the higher order polynomial coefficients b_1 and b_2 should model the observed microlensing chromaticity. We fit the data using the Cardelli et al. (1989, hereafter CCM) and Fitzpatrick & Massa (1990, hereafter FM) multi-parametric models for R_λ.

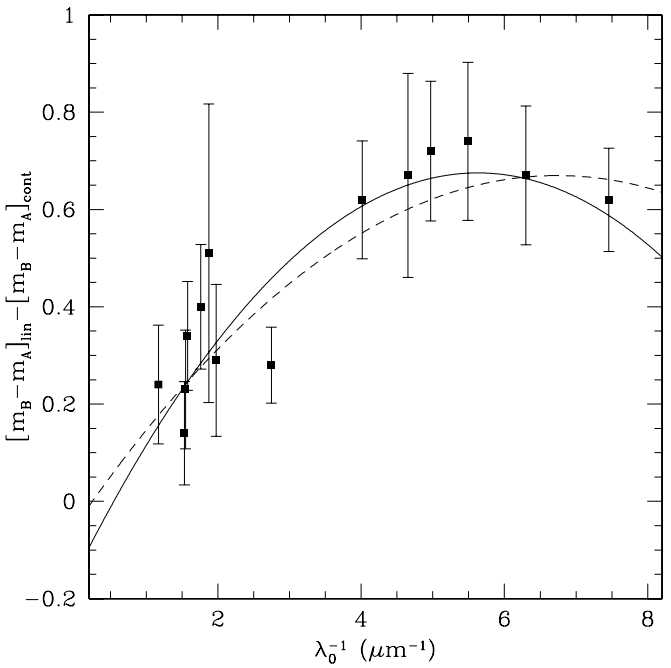

Figure 7. Squares: microlensing magnification data inferred from the ratios between continuum and emission line fluxes. Solid line: ratio between the fits based on the Fitzpatrick & Massa (1990) models with and without microlensing chromaticity (see the text). Dashed line: second order in λ^{-1} polynomial fit to the microlensing magnification data.

The latter model is able to account for the extinction observed in a broader range of environments (see Gordon et al. 2003). Figure 5 shows the results with no chromaticity ($b_1 \equiv b_2 \equiv 0$) and Figure 6 shows the results corresponding to the FM model when the continuum chromaticity is a quadratic function of λ^{-1}. In each case we did the fits both for the dust at the lens redshift ($z_d = z_l = 0.83$) and allowing it to vary. In all the fits the 2175 Å feature is clearly required and the dust redshift estimate $z_d = 0.83 \pm 0.01$ is consistent with the spectroscopic redshift. We find that the CCM model (Figure 5) fails to fit the bump well. As previously noted by Mediavilla et al. (2005), the preferred model is similar to the dust in the LMC2 Supershell. Note, however, that the CCM model is a better fit in the near-IR because in the FM parameterization the extinction is simply λ^{-1} in this region. In Figure 7 we show how the difference between the fits, with and without microlensing chromaticity, follows the microlensing magnification data (a second order polynomial directly fitted to the microlensing data is included in this figure to show the consistency of the procedure).

4. CONCLUSIONS

We have clearly detected chromatic microlensing in SBS 0909+532 by comparing the B/A flux ratios of 14 emission lines and of their underlying continua over a spectral region ranging from the near-IR to the far-UV. The microlensing magnification is highest in the UV (-0.67 ± 0.05 at ~1500 Å) and smoothly diminishes toward the IR (-0.24 ± 0.07 at ~6600 Å). To explain this large chromaticity, image B should be in a region of high magnification, likely crossing or very close to a caustic. This is the case in 90% of our simulations. However, comparison with optical and near-IR (but not UV) broadband data from the literature taken at two different epochs separated by ~9 and ~6 years from our observations shows no significant time variability.

Using a Bayesian analysis we have estimated the disk size, modeled as a Gaussian of dispersion r_s, and the power-law index, p, relating the disk sizes at different wavelengths, $r_s \propto \lambda^p$, needed to explain the observed chromaticity. The estimated half-light radius of 4–8 light-days at $\lambda_{\rm rest} \sim 1500$ Å, depending on the priors, is in reasonable agreement with the size estimated using thin disk theory and the black hole mass estimated from the emission line widths ($R_{1/2} \sim 2.4$ light-days), but not with the smaller size estimated from the optical flux ($R_{1/2} \sim 1$ light-days). The estimate of the size scaling index, $p = 0.9^{+0.6}_{-0.3}$, is compatible with the temperature profile of a thin disk model ($T \propto R^{-3/4} \propto R^{-1/p}$, that is, $p = 4/3$).

The separation of extinction and microlensing effects using the emission line flux ratios is straightforward and consistent and, in any case, microlensing chromaticity does not significantly affect the determination of the dust redshift or the characterization of the 2175 Å bump parameters from the magnitude difference curves. We have used the Fitzpatrick & Massa analytical model to fit the extinction law curve confirming the differences noted by Mediavilla et al. (2005) between the extinction law in the lens galaxy of SBS 0909+532 and that of the Milky Way. The best-fitting extinction curve is similar to that of the LMC2 Supershell.

Based on observations with the NASA/ESA *Hubble Space Telescope*, which is operated by the Association of Universities for Research in Astronomy, Inc., under NASA contract NAS 5-26555. This research was supported by the European Community's Sixth Framework Marie Curie Research Training Network Programme, Contract No. MRTN-CT-2004-505183 "ANGLES," and by the Spanish Ministerio de Educación y Ciencias (grants AYA2004-08243-C03-01/03 and AYA2007-67342-C03-01/03). J.A.M. is also supported by the Generalitat Valenciana with the grant PROMETEO/2009/64. C.S.K. is supported by NSF grants AST-0708082 and AST-1009756. V.M. acknowledges the partial support of grant FONDECYT 1090673. J.A.A.P. and A.M.T. are partially supported by the Spanish MICINN grant AYA2004-03136. A.M.M. acknowledges the support of Generalitat Valenciana, grant APOSTD/2010/030.

REFERENCES

Abajas, C., Mediavilla, E., Muñoz, J. A., Popović, L. Č., & Oscoz, A. 2002, ApJ, 576, 640
Agol, E., Gogarten, S. M., Gorjian, V., & Kimball, A. 2009, ApJ, 697, 1010
Anguita, T., Schmidt, R. W., Turner, E. L., Wambsganss, J., Webster, R. L., Loomis, K. A., Long, D., & McMillan, R. 2008, A&A, 480, 327
Arribas, S., et al. 1998, Proc. SPIE, 3355, 821
Assef, R. J., et al. 2010, ApJ, 713, 970
Bate, N. F., Floyd, D. J. E., Webster, R. L., & Wyithe, J. S. B. 2008, MNRAS, 391, 1955
Blackburne, J. A., Pooley, D., Rappaport, S., & Schechter, P. L. 2010, arXiv:1007.1665
Bonning, E. W., Cheng, L., Shields, G. A., Salviander, S., & Gebhardt, K. 2007, ApJ, 659, 211
Cardelli, J. A., Clayton, G. C., & Mathis, J. S. 1989, ApJ, 345, 245
Chang, K., & Refsdal, S. 1979, Nature, 282, 561
Dai, X., Kochanek, C. S., Chartas, G., Kozłowski, S., Morgan, C. W., Garmire, G., & Agol, E. 2010, ApJ, 709, 278
Eigenbrod, A., Courbin, F., Meylan, G., Agol, E., Anguita, T., Schmidt, R. W., & Wambsganss, J. 2008, A&A, 490, 933
Fabian, A. C. 2005, Ap&SS, 300, 97
Falco, E. E., et al. 1999, ApJ, 523, 617
Fitzpatrick, E. L., & Massa, D. 1990, ApJS, 72, 163
Floyd, D. J. E., Bate, N. F., & Webster, R. L. 2009, MNRAS, 398, 233
Gaskell, C. M. 2008, Rev. Mex. Astron. Astrofis. Conf. Ser., 32, 1
Gordon, K. D., Clayton, G. C., Misselt, K. A., Landolt, A. U., & Wolff, M. J. 2003, ApJ, 594, 279
Jaroszynski, M., Wambsganss, J., & Paczynski, B. 1992, ApJ, 396, L65
Kochanek, C. S. 2004, ApJ, 605, 58
Kochanek, C. S. 2006, in Gravitational Lensing: Strong, Weak and Micro, Saas-Fee Advanced Courses, Vol. 33, ed. G. Meylan, P. Jetzer, & P. North (Berlin: Springer), 91
Kochanek, C. S., Falco, E. E., Schild, R., Dobrzycki, A., Engels, D., & Hagen, H.-J. 1997, ApJ, 479, 678
Lehár, J., et al. 2000, ApJ, 536, 584
Manchado, A., et al. 2004, Proc. SPIE, 5492, 1094
Mediavilla, E., Muñoz, J. A., Kochanek, C. S., Falco, E. E., Arribas, S., & Motta, V. 2005, ApJ, 619, 749
Mediavilla, E., Muñoz, J. A., Lopez, P., Mediavilla, T., Abajas, C., Gonzalez-Morcillo, C., & Gil-Merino, R. 2006, ApJ, 653, 942
Mediavilla, E., et al. 2009, ApJ, 706, 1451
Morgan, C. W., Kochanek, C. S., Dai, X., Morgan, N. D., & Falco, E. E. 2008, ApJ, 689, 755
Morgan, C. W., Kochanek, C. S., Morgan, N. D., & Falco, E. E. 2010, ApJ, 712, 1129
Mosquera, A. M., Muñoz, J. A., & Mediavilla, E. 2009, ApJ, 691, 1292
Motta, V., et al. 2002, ApJ, 574, 719
Muñoz, J. A., Falco, E. E., Kochanek, C. S., McLeod, B. A., & Mediavilla, E. 2004, ApJ, 605, 614
Nadeau, D., Yee, H. K. C., Forrest, W. J., Garnett, J. D., Ninkov, Z., & Pipher, J. L. 1991, ApJ, 376, 430
Oscoz, A., Serra-Ricart, M., Mediavilla, E., Buitrago, J., & Goicoechea, L. J. 1997, ApJ, 491, L7
Peng, C. Y., Impey, C. D., Rix, H.-W., Kochanek, C. S., Keeton, C. R., Falco, E. E., Lehár, J., & McLeod, B. A. 2006, ApJ, 649, 616
Poindexter, S., & Kochanek, C. S. 2010, ApJ, 712, 668
Poindexter, S., Morgan, N., & Kochanek, C. S. 2008, ApJ, 673, 34
Pooley, D., Blackburne, J. A., Rappaport, S., & Schechter, P. L. 2007, ApJ, 661, 19
Rauch, K. P., & Blandford, R. D. 1991, ApJ, 381, L39
Salpeter, E. E. 1964, ApJ, 140, 796
Sergeev, S. G., Doroshenko, V. T., Golubinskiy, Y. V., Merkulova, N. I., & Sergeeva, E. A. 2005, ApJ, 622, 129
Shakura, N. I., & Sunyaev, R. A. 1973, A&A, 24, 337
Wambsganss, J. 2006, in Gravitational Lensing: Strong, Weak and Micro, Saas-Fee Advanced Courses, Vol. 33, ed. G. Meylan, P. Jetzer, & P. North (Berlin: Springer), 453
Wisotzki, L., Koehler, T., Ikonomou, M., & Reimers, D. 1995, A&A, 297, L59
Wisotzki, L., Koehler, T., Kayser, R., & Reimers, D. 1993, A&A, 278, L15
Wucknitz, O., Wisotzki, L., Lopez, S., & Gregg, M. D. 2003, A&A, 405, 445
Yonehara, A., Mineshige, S., Manmoto, T., Fukue, J., Umemura, M., & Turner, E. L. 1998, ApJ, 501, L41
Zel'Dovich, Y. B. 1964, Sov. Phys. Dokl., 9, 195